



HAL
open science

Low frequency noise analysis on Si/SiGe superlattice I/O n-channel FinFETs

D. Boudier, B Cretu, E. Simoen, G. Hellings, T. Schram, H. Mertens, D.
Linten

► **To cite this version:**

D. Boudier, B Cretu, E. Simoen, G. Hellings, T. Schram, et al.. Low frequency noise analysis on Si/SiGe superlattice I/O n-channel FinFETs. Solid-State Electronics, 2019, pp.107732. 10.1016/j.sse.2019.107732 . hal-02438740

HAL Id: hal-02438740

<https://hal.science/hal-02438740>

Submitted on 20 May 2022

HAL is a multi-disciplinary open access archive for the deposit and dissemination of scientific research documents, whether they are published or not. The documents may come from teaching and research institutions in France or abroad, or from public or private research centers.

L'archive ouverte pluridisciplinaire **HAL**, est destinée au dépôt et à la diffusion de documents scientifiques de niveau recherche, publiés ou non, émanant des établissements d'enseignement et de recherche français ou étrangers, des laboratoires publics ou privés.



Distributed under a Creative Commons Attribution - NonCommercial 4.0 International License

Low frequency noise analysis on Si/SiGe superlattice I/O n-channel FinFETs

D. Boudier¹, B. Cretu¹, E. Simoen^{2,3}, G. Hellings², T. Schram², H. Mertens², and D. Linten²

¹Normandie Univ, UNICAEN, ENSICAEN, CNRS, GREYC, 14000 Caen

²Imec, Kapeldreef 75, B-3001 Leuven, Belgium

³Solid-State Physics Department, Ghent University, 9000 Gent, Belgium

e-mail: bogdan.cretu@ensicaen.fr

Corresponding author: Bogdan Cretu

e-mail: bogdan.cretu@ensicaen.fr

Tel: +33 (0) 2 31 45 27 17

Fax: +33 (0) 2 31 45 26 98

Low frequency noise analysis on Si/SiGe superlattice I/O n-channel FinFETs

Abstract

Low frequency noise studies are performed in Si/SiGe superlattice I/O n-channel FinFETs. It was observed that the experimental noise spectra may contain additionally to flicker and white noise one or several generation recombination (GR) components. The methodology to estimate the noise parameters corresponding to the $1/f$ noise and each GR noise contribution was detailed. It is found that the carrier number fluctuations mechanisms prevail the $1/f$ noise. The important $1/f$ noise level variability observed for devices having the same geometry may be related to the remote Coulomb scattering effect through the correlation between the mobility and the $1/f$ noise levels. Low frequency noise spectroscopy was performed allowing to identify traps related to divacancies, hydrogen and a possible carbon contamination in Si/SiGe fins.

I. Introduction

Fully depleted and multiple gate MOSFETs are the best candidates for the ultimate CMOS technologies below 5 nm node. In the framework of a study initiated to compare in particular the noise performances between superlattice FinFETs and gate all around nanowires (GAA NWs) designed using the same process flow, with some additional steps for nanowires, in this work preliminary low frequency noise (LFN) results obtained on Si/SiGe superlattice Input/Output (I/O) n- channel devices are shown.

The investigated devices, fabricated at imec on 300 mm silicon wafers present a fin width of 10 nm, a fin height of 10 nm and four fins in parallel, leading to an equivalent channel width of 120 nm. As the gate oxide stack includes 2 nm high-k dielectric (HfSiO) on top of a 5 nm interfacial SiO₂, an equivalent oxide thickness (EOT) of 5.6 nm is considered. A complete description of the devices fabrication flow is provided in [1]. **Details on the experimental set-up are given in [2].**

In the second section, the methodology to extract the **LFN** parameters, in particular the $1/f$ noise level and the plateau and the characteristic frequency of the GR component is fully described through a noise spectrum example which contains several GR components .

In the third section, the low frequency noise as a function of the applied gate voltage is firstly characterized at room temperature in order to investigate the quality of the oxidation process using the $1/f$ noise analysis. LFN measurements as a function of the temperature at fixed drain current polarisation are effectuated in order to have information on the quality of the depleted Si film. This preliminary LFN spectroscopy investigation allows to identify several processing induced traps.

II. Methodology for LFN parameters estimation

The **input-referred** gate voltage noise (S_{vg}) may be modelled assuming that the noise power spectral density contains contributions of three uncorrelated noise sources: white noise, flicker noise and GR noise. The white noise is independent on the frequency (in particular in the low frequency range), the flicker noise decreases with the increase of the frequency and the GR noise is characterised by a plateau and a characteristic frequency. The input-referred S_{vg} power spectral density can be written as follow (e.g. equation 6 of [3]):

$$S_{v_g}(f) = \frac{S_{id}}{g_m^2} = W_n + \frac{K_f}{f} + \sum_{i=1}^N \frac{A_i}{1 + \left(\frac{f}{f_{0i}}\right)^2} \quad (1)$$

This model - equation can be successfully used to estimate the $1/f$ noise levels (noted K_f and corresponding to the $1/f$ noise level at a frequency of 1 Hz), the white noise level (W_n) and the characteristic frequency (f_{0i}) and the plateau (A_{oi}) of the GR noise contributions for all measured noise spectra, in particular when the input-referred noise is multiplied by the frequency. Indeed, in $S_{vg} \cdot f$ representation, the flicker noise will present a plateau giving the K_f level, and each GR contribution will be represented by bumps centred at their characteristic frequencies. The slope of the linear increase of the $S_{VG} \cdot f$ with the frequency in the highest frequency range **consistently** gives the white noise level.

An example of a noise spectrum containing several GR contributions is presented in Figure 1a.

In a first step input values for the plateau and the characteristic frequency corresponding to the most pronounced GR contribution, in our case in the highest investigated frequencies, are obtained. For the maximum of the bump, the estimation of the characteristic frequency may be made ($f_{01} \approx 6700$ Hz). In first **approximation**, it is considered that:

- the other GR contributions have limited impact on the behaviour of the first considered GR contribution;
- the flicker noise is firstly considered as the mean value of $S_{VG} \cdot f$ at $f = 1$ Hz (i.e. $3 \cdot 10^{-7}$ V²), and so it can be neglected;
- the white noise may be in first **approximation** also neglected as no clear increase of the $S_{VG} \cdot f$ may be observed in the highest frequency range (around 100 kHz),.

In these conditions, at $f = f_{01}$ Equation 1 becomes:

$$S_{v_g}(f_{01}) \cdot f_{01} \approx \frac{A_1 \cdot f_{01}}{2} \quad (2)$$

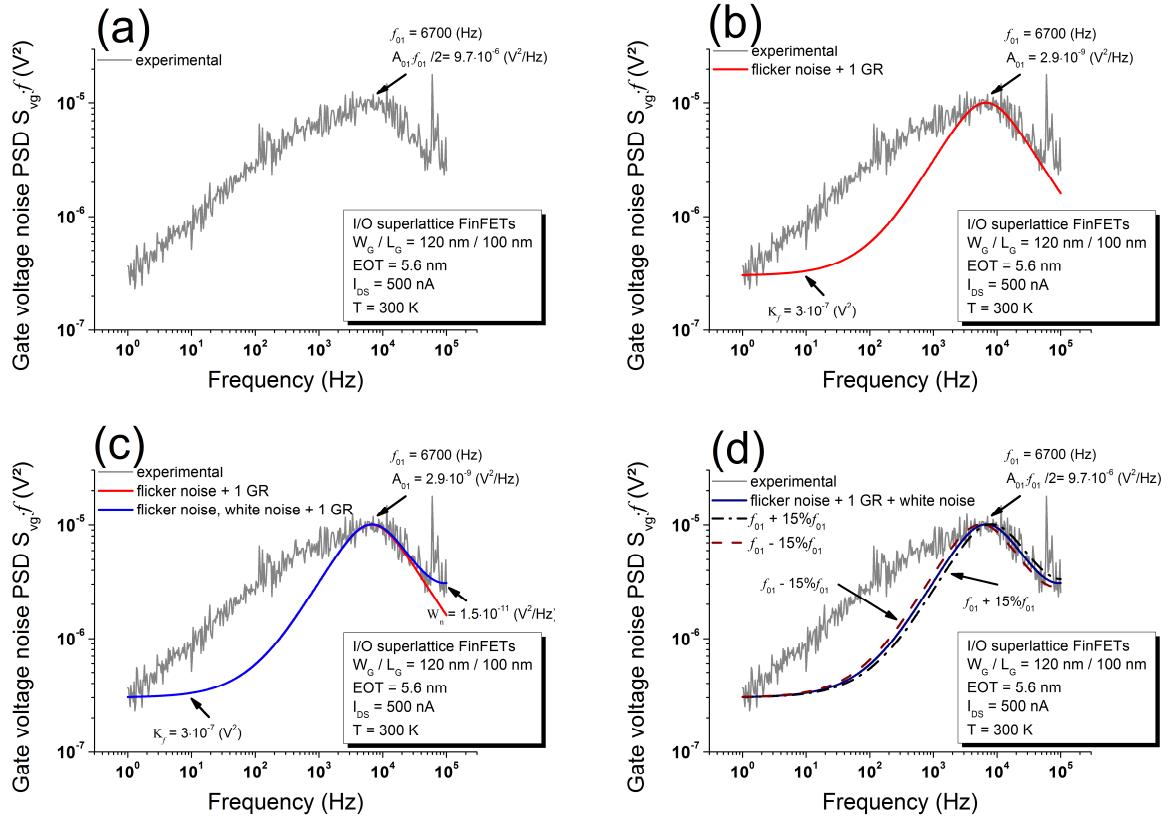


Figure 1. a) example of a noise spectrum containing several GR contributions; b) model using f_{01} from the maximum of the bump and A_{01} from equation 2; c) adjusting the model by considering the white noise contribution (no impact on the A_{01} estimation may be observed); d) Estimation error of about $\pm 15\%$ on f_{01} does not allow a good fit to the spectrum for frequencies higher than f_{01} .

For the maximum of the bump (mean value of $S_{VG}; f_{01} \approx 9.7 \cdot 10^{-6} \text{ V}^2$) an input value of about $2.9 \cdot 10^{-9} \text{ V}^2/\text{Hz}$ of the plateau of the first GR contribution considered may be obtained. Using these values for f_{01} and A_{01} , it may be observed that the noise spectrum is not well fitted for frequencies close to 100 kHz (Figure 1b). Consequently, the white noise contribution should be considered. Using a value of $1.5 \cdot 10^{-11} \text{ V}^2/\text{Hz}$ a good agreement between the experimental data and model can be observed for frequencies higher than f_{01} (Figure 1c). As can be observed from Figure 1d, the admitted error on f_{01} estimation should be less than 15% (f_{01} adjusted with respect of (2)). One can suggest that f_{01} may be taken as $(f_{01\text{max}} - f_{01\text{min}})/2$, where $f_{01\text{min}}$ and $f_{01\text{max}}$ are the minimum and the maximum values for which the noise spectra could be considered well fitted.

The same strategy is used for the second GR contribution. However, because the GR contributions are relatively close to each other, A_{01} and A_{02} may be adjusted in order to have a better fitting. A reduction with less than 10% from A_{01} should be made (Figure 2a). Variation of the f_{02} with $\pm 15\%$ leads to a clear disagreement between the experimental curves and the model (Figure 2b).

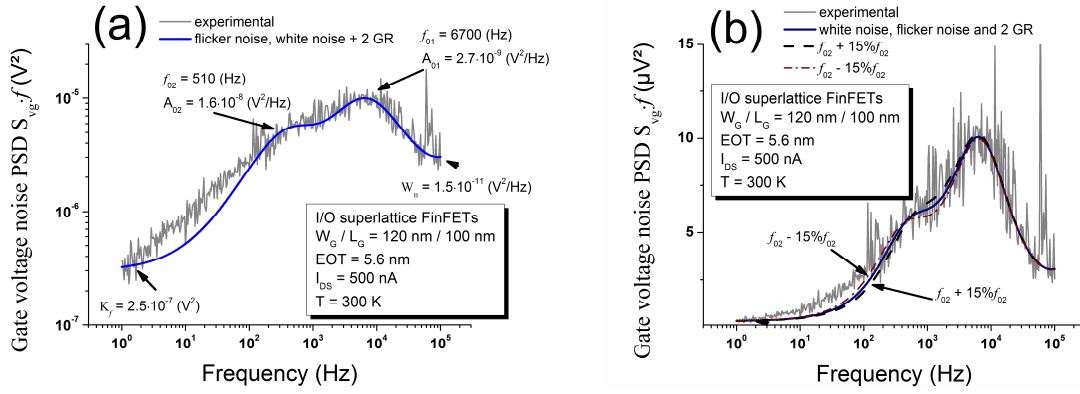


Figure 2: a) model of (1) using flicker noise, white noise and two GR contributions, b) disagreement if about $\pm 15\%$ variation is considered for the input f_{02} value. Better view may be obtained if a linear scale is chosen for the Oy-axis.

Finally, input values for the third GR contribution are given and an adjustment for the flicker noise is made (Figure 3a). In the very low frequency range for which it may be assumed that the impact of the first, second Lorentzian and of the white noise contributions may be neglected and for which $(f/f_{03})^2 \ll 1$ Considering these hypotheses, Equation 1 may be simplified as:

$$S_{v_g}(f) \cdot f \approx K_f + \frac{A_3 \cdot f}{1 + \left(\frac{f}{f_{03}}\right)^2} \approx K_f + A_3 \cdot f \quad (3)$$

Using the $S_{v_g}(f) \cdot f$ values for different frequencies for which the considered hypotheses are fulfilled, the given input values for f_{03} and A_{03} can be also verified. The results by using three different very low frequencies are summarized in Table 1.

Table 1. A_{03} and K_f estimation using first order approximations in Equation 1, considering three different frequencies in Equation 3

f (Hz)	$S_{v_g} \cdot f$ (V ²)	A_{03} (V ² /Hz)	K_f (V ²)
1	$3 \cdot 10^{-7}$	$4 \cdot 10^{-8}$	$2.3 \cdot 10^{-7}$
2	$3.7 \cdot 10^{-7}$	$5 \cdot 10^{-8}$	$2.3 \cdot 10^{-7}$
4	$4.5 \cdot 10^{-7}$	$4 \cdot 10^{-8}$	$2.9 \cdot 10^{-7}$

A good agreement between the experimental noise spectrum and model is observed, except for the 3 -10 Hz frequency range (Figure 3a). Further, a fourth GR contribution at f_{04} of about 4 Hz and a last adjustment of the K_f level may be performed in order to have a best fitting of the experimental noise (Figure 3b). However, as this last GR contribution has a very limited impact on the estimation of A_{01} , f_{01} , A_{02} , f_{02} , A_{03} , f_{03} and W_n noise parameters, it affects principally the flicker noise level.

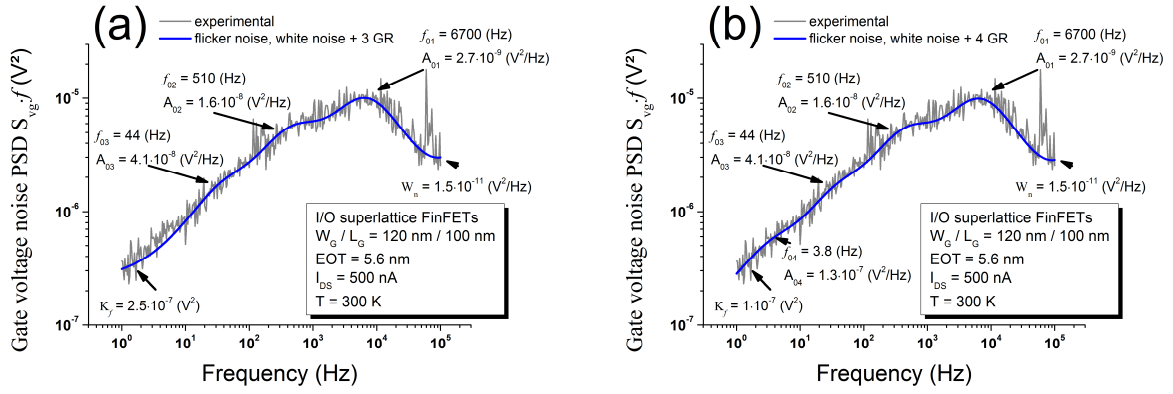


Figure 3: a) model of (1) using flicker noise, white noise and three GR contributions; b) best fit if in the model of (1) flicker noise, white noise and four GR contributions are considered

However, for other examples the LFN parameter estimation is made more **easy**, as observed from Figure 4 for device 1, where only a white noise and flicker noise contribution should be considered to obtain good agreement between the experimental and modelled spectrum. The K_f level is estimated in the frequency range where a plateau may be observed (i.e. 1 Hz – 1 kHz), while the white noise level is given using the frequency range in which a direct proportional evolution between $S_g(f) \cdot f$ and the frequency may be observed (i.e. 10 kHz - 100 kHz). In the same polarisation conditions, two GR contributions may additionally be taken in consideration for device 3.

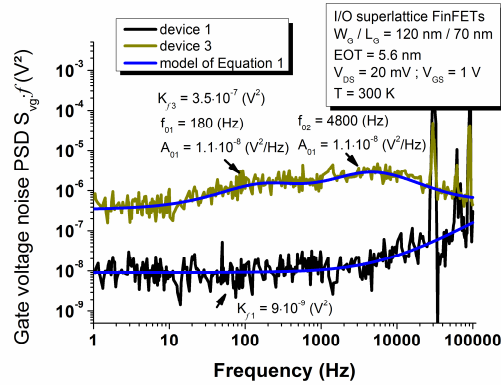


Figure 4. Experimental noise spectra for devices having the same geometry.

III. Results and discussion

A. LFN at room temperature

LFN measurements are performed at room temperature for several devices having the same geometry. Typical example of the estimated K_f behaviour versus the applied gate voltage overdrive V_{GT} ($V_{GT} = V_{GS} - V_{t_{ext}}$, $V_{t_{ext}}$ being the threshold voltage) for two samples having the same mask gate length of 70 nm is plotted in Figure 5.

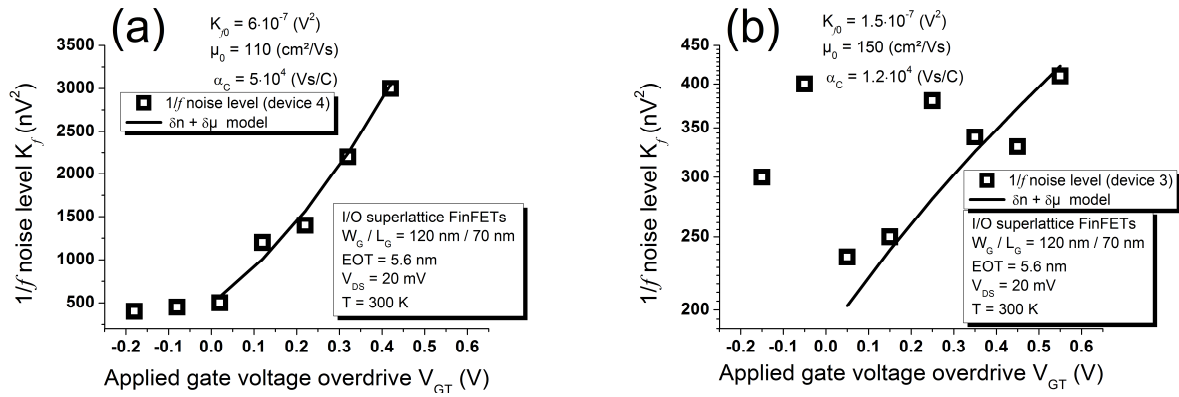


Figure 5. Estimated 1/f noise level evolution with the applied gate voltage. The increase of the K_f level after threshold may be perfectly model in the framework of the carrier number fluctuations correlated to mobility fluctuations model

The quasi-independence of the K_f level with the applied V_{GT} close to the threshold (Figure 5a) suggests that the carrier number fluctuations mechanism prevails the flicker noise. The increase of the K_f level with the applied gate voltage after the threshold may be related to the carrier number fluctuations correlated to mobility fluctuations mechanism (δn + δμ) and may be modelled as [4]:

$$K_f = \frac{q^2 k_B T \lambda N_{it}}{W L C_{ox}^2} (1 + \alpha_C \mu_0 C_{ox} V_{GT})^2 = K_{f0} (1 + \alpha_C \mu_0 C_{ox} V_{GT})^2 \quad (4)$$

where k_B is the Boltzmann constant, T is the temperature, N_{it} is the density of traps in the gate dielectrics at the quasi-Fermi level (cm⁻³eV⁻¹), λ is the tunnel distance, μ₀ is the low field mobility, C_{ox} the is the gate oxide capacitance, α_C is the Coulomb scattering coefficient and K_{f0} represent the flat-band noise level (S_{vfb}) at 1 Hz. A good correlation between the δn + δμ model and the 1/f noise behaviour presented in Figure 5a may be observed. Using the low field mobility extracted in first approximation from the maximum of the transconductance, a value of α_C of 5·10⁴ Vs/C is obtained.

From Figure 5b, considering only the values after threshold such good agreement may be observed between the K_f versus V_{GT} and the δn + δμ model, leading to a value of α_C of about 1.2·10⁴ Vs/C. Considering the low field

mobility and α_C values obtained for devices 3 and 4 it may be suggested that the low field mobility reduction may be linked to the increase of the Coulomb interactions.

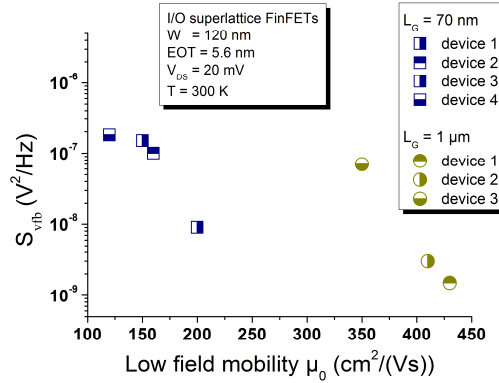


Figure 6. Extracted flat-band noise levels versus low field mobility

Equation (4) permits to determine the volume trap density from the estimated K_{f0} levels for each studied device. The surface trap density D_{it} can be extracted as in [4,5] using the expression $D_{it} = 4 k_B T z N_{it}$, where z is the tunnelling distance in the depth of oxide taken at a frequency of 1 Hz.

In Figure 6 are plotted the estimated flat-band $1/f$ noise levels versus the corresponding low field mobility for all investigated devices. A substantial variability of S_{vfb} of more than one decade can be observed. It may be noted that the S_{vfb} is always higher for devices presenting lower low field mobility. The correlation between the $1/f$ noise levels and the mobility has been already reported in the literature for other technologies and was related to remote Coulomb scattering [4,5]. This hypothesis corroborates with the results of Figure 5.

B. LFN as a function of the temperature

Following the arguments proposed by [7], if the evolution of the characteristic frequency of the GR noise contribution is independent on the applied gate voltage at fixed temperature operation and varies with temperature at fixed polarisation operation condition, than it can be related to traps located in the Si fins. In order

to keep a quasi-constant Fermi level, the LFN measurements as the function of the temperature should be made at fixed drain current polarisation.

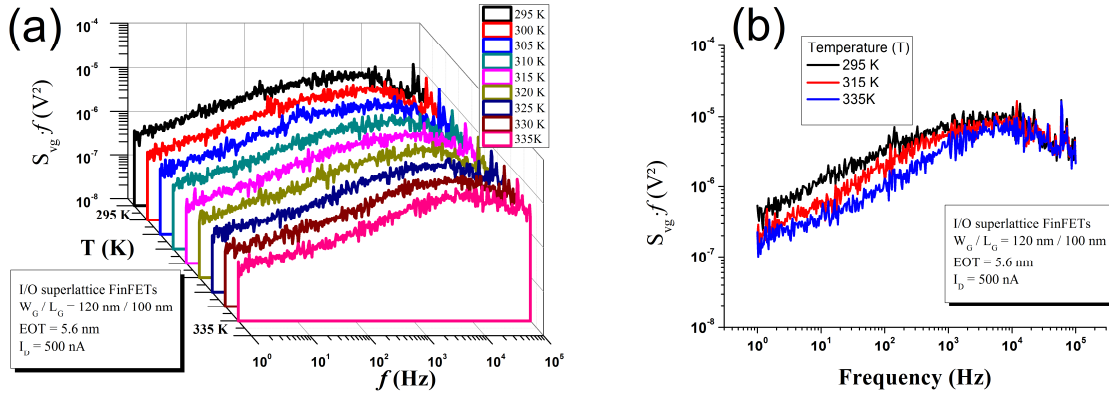


Figure 1 Input-referred PSD noise multiplied by frequency evolution with the temperature

This first low frequency noise spectroscopy study is made for a 100 nm gate length device operated at fixed polarization of 500 nA. The investigated temperature (T) window is from 295 K to 335 K, using a temperature step of 5 K. The temperature evolution of input-referred gate voltage noise multiplied by the frequency $S_{vg}f$ is plotted in Figure 1. The characteristic frequency and plateau of each GR contributions are estimated using the methodology presented in section III. The estimation error on the characteristic frequencies of GR noise is taken using $f_{0i\min}$ and f_{0imax} for each GR contribution, where $f_{0i\min}$ and f_{0imax} are the minimum and the maximum values for which the noise spectra could be considered well fitted. The PSD was always verified in time domain representation.

The Arrhenius diagrams presented in Figure 2 are constructed using the method proposed in [7,8], which consists to plot the variations of $\ln(\tau_i T^2)$ as a function of $1/k_B T$, where τ_i is the characteristic relaxation time ($\tau_i = 1/(2\pi f_{0i})$) and k_B is the Boltzmann constant. The energy difference between the conduction band energy (E_C) and the trap energy E_T and the capture cross-section σ_n could be extracted from the slope and the y-intercept, respectively (least-squares linear fit to the data). The physical nature of the identified traps is based on a comparison with previous results from Deep-Level Transient Spectroscopy (DLTS) studies [9-12]. The $E_C - E_T$ and σ_n issued from the Arrhenius diagram presented in Figure 8 are summarized in Table 2.

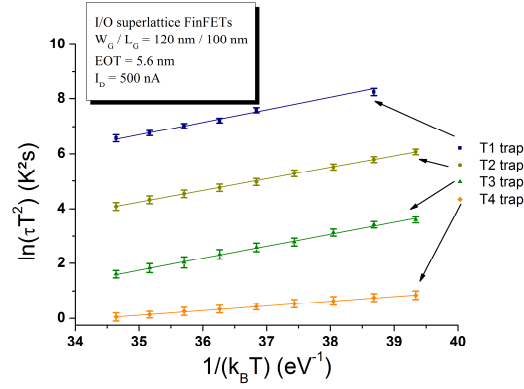


Figure 1. Arrhenius diagram constructed using the method proposed in [7,8].

Table 2. Summary of the estimated noise parameters of the identified traps.

	$\Delta E = E_C - E_T$ (eV)	σ_n (cm ²)	T (K)	N_{eff} (cm ⁻²)
T1	0.452 ± 0.013	$(0.1 - 0.8) \cdot 10^{-17}$	315 – 335	$6.2 \cdot 10^{10}$
T2	0.4206 ± 0.005	$(0.08 - 0.12) \cdot 10^{-16}$	295 – 335	$22 \cdot 10^{10}$
T3	0.438 ± 0.01	$(0.16 - 0.3) \cdot 10^{-15}$	295 – 335	$8.5 \cdot 10^{11}$
T4	0.1708 ± 0.005	$(0.9 - 1.2) \cdot 10^{-19}$	295 – 335	$2.8 \cdot 10^{12}$

The first trap observed (noted T1) presents a ΔE and capture cross-section close to those reported in the literature for the divacancy-hydrogen V_2H trap (ΔE of 0.45 eV and a σ_n in the 10^{-17}cm^2 range [9,10]). The V_2H trap may be due to the presence of residual hydrogen after annealing.

The extracted activation energy for the T2, T3 traps suggests the impact of the single negatively charged acceptor state (0/-) of the divacancy (V_2) trap (i.e. ΔE of 0.42 eV) and the phosphorus-vacancy complex (V-P) (i.e. 0.44 eV), respectively [9,11]. However, the capture cross-section is smaller than expected (e.g. σ_n in the range of 10^{-15}cm^2 for both the $V_2(0/-)$ and V-P traps). The presence of these two divacancies may be explained by the recombination or the evolution to a stable state of the unstable defects like Frenkel pairs, which could be generated during ion implantation.

Concerning T4, the same activation energy of 0.17 eV is reported for traps related to the oxygen - vacancy complex V-O and for the interstitial – carbon – substitutional carbon complex C_iC_s [9,12]. The reported σ_n for V-O is reported in the range of 10^{-14}cm^2 [12], while no value for the capture cross-section of the C_iC_s complex is reported to our knowledge. Even if the C_iC_s complex is reported to be improbable, considering the extracted values of σ_n in the range of 10^{-19}cm^2 it is more likely that T4 is related to the C_iC_s complex.

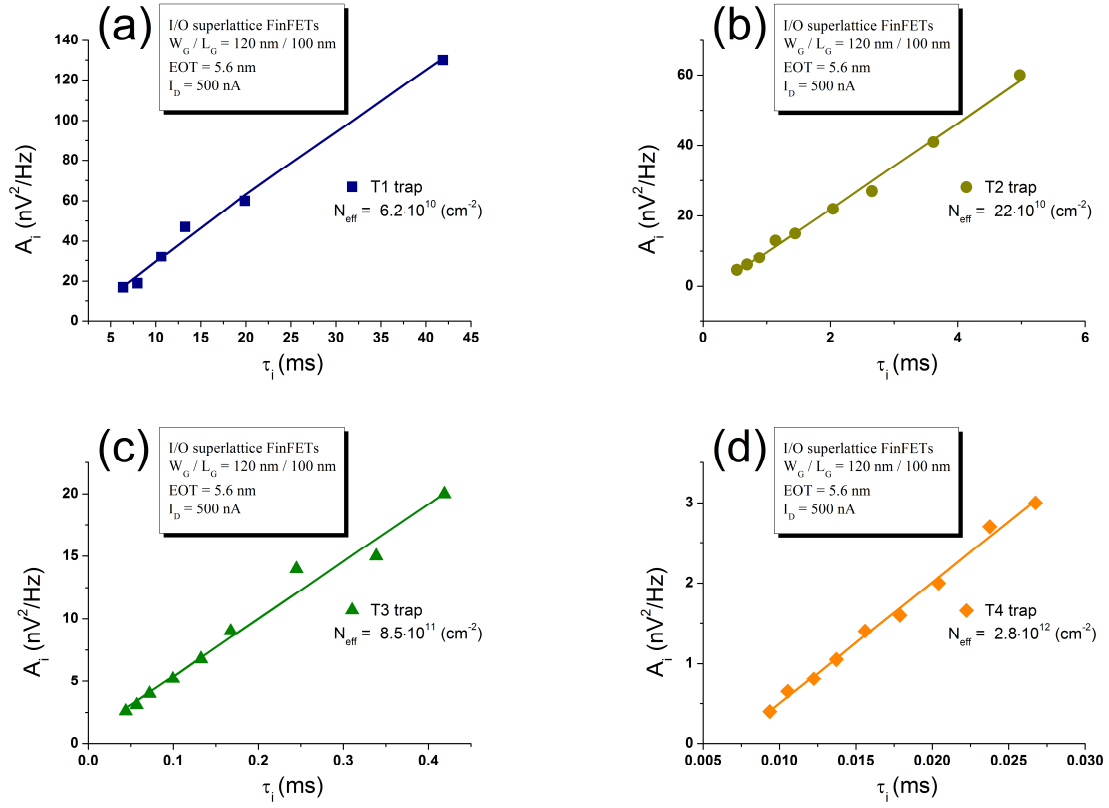


Figure 1. A linear dependencies between the GR plateau A_{0i} versus the characteristic relaxation time τ_{0i} exists, confirming that A_{0i} and τ_{0i} are related to the same trap

The relationship between the GR plateau and the GR characteristic time constant may be used as a second verification step for trap validation. Indeed, a linear dependence should exist between A_{0i} and τ_{0i} related to the same trap. This linearity is verified for all identified traps, as can be observed in Figure 1. Moreover, from the slope of A_{0i} versus τ_{0i} the effective surface density of the traps may be evaluated without any additional assumption. Indeed, for the estimation of the volume trap density in conventional planar devices a correction parameter (B) value of 1/3 should be considered [7]. However, it was already demonstrated that this B parameter value is no longer a constant for multiple-gate devices [3,13]. The obtained values of the surface trap density of the identified traps, summarized in Table 2 are moderately larger compared to those previously reported for other advanced technologies [13,14].

IV. Conclusions

The noise parameters estimation protocol was fully described for a PSD noise which contains several GR noise contributions.

The evolution of the $1/f$ noise levels with applied bias confirms that the carrier number fluctuation mechanism explains the flicker noise origin in the studied Si/SiGe superlattice FinFETs. The correlation between the mobility and the $1/f$ noise levels related to the remote Coulomb scattering effect explains the important $1/f$ noise level variability.

Taking into account the estimation error of the GR noise parameters, the analysis of the temperature evolution of the characteristic frequency and plateau of each GR contribution permits to identify the presence of traps located in the depleted Si film related to divacancies, hydrogen and a possible carbon contamination. The linear dependencies between the GR plateau A_{0i} versus the characteristic relaxation time τ_{0i} additionally confirms the trap identification.

REFERENCES

- [1] G. Hellings, H. Mertens, A. Subirats, E. Simoen, T. Schram, L.-A. Ragnarsson *et al.*, "Si/SiGe superlattice I/O finFETs in a vertically-stacked Gate-All-Around horizontal Nanowire Technology" in Tech. Dig. Symp. on VLSI Technology, The IEEE New York, 2018, p.p. 85-86, DOI: 10.1109/VLSIT.2018.8510654.
- [2] D. Boudier, B. Cretu, E. Simoen, R. Carin, A. Veloso, N. Collaert, and A. Thean, "Low frequency noise assessment in n- and p-channel sub-10 nm triple-gate FinFETs: Part I: Theory and methodology," Solid State Electron., vol. 128, pp. 102-108, 2017, DOI: 10.1016/j.sse.2016.10.012.
- [3] H. Achour, B. Cretu, E. Simoen, J.-M. Routoure, R. Carin, A. Benfdila, M. Aoulaiche and C. Claeys., "Identification of Si film traps in p-channel SOI FinFETs using low temperature noise spectroscopy", Solid-State Electron 2015; 112, pp 1-6, DOI: 10.1016/j.sse.2015.02.014.
- [4] G. Ghibaud, O. Roux, Ch. Nguyen-Duc, F. Balestra and J. Brini., "Improved analysis of low frequency noise in field-effect MOS transistors" Phys. Stat. Sol. (a), vol. 124, no. 2, pp. 571-581, 1991, DOI: 10.1002/pssa.2211240225
- [5] W. Guo, G. Nicholas, B. Kaczer, R. M. Todi, C. Claeys, A. Mercha, E. Simoen *et al.*, "Low-frequency noise assessment of silicon passivated Ge pMOSFETs with TiN/TaN/ HfO₂ gate stack" IEEE Electron Device Letters 2007; vol. 28, 4, pp 288-291, DOI: 10.1109/LED.2007.891797
- [6] E. Simoen, A. Mercha and C. Claeys., "Correlation between the $1/f$ noise parameters and the low-field mobility in HfO₂ gate dielectric n-channel metal-oxide-semiconductor field-effect transistors" Appl. Phys Lett., 2004, pp 1057-1059, DOI: 10.1063/1.1779967
- [7] N. Lukyanchikova, "Noise and Fluctuations Control in Electronic Device" edited by A. Balandin American Scientific, Riverside, CA 2002, pp. 201-233.
- [8] V. Grassi, C.F. Colombo and D.V. Camin, "Low frequency noise versus temperature spectroscopy of recently designed Ge JFETs", IEEE Trans. Electron Dev., 2001, 48, pp. 2899- 2905, DOI: 10.1109/16.974725
- [9] C. Claeys and E. Simoen, "Radiation effects in Advanced Semiconductor Material and Devices", Springer Verlag, 2002.
- [10] A. Hallen, N. Keskitalo, F. Masszi, and V. Nagl. "Lifetime in proton irradiated silicon", J. Appl. Phys., 1996, 79 (8), pp. 3906 – 14, DOI: 10.1063/1.361816.
- [11] J.A. van Vechten, "Vacancies, dislocations, and carbons interstials in Si", Phys. Rev. B, 197,; 35(2), pp. 864- 80. DOI: 10.1103/PhysRevB.35.864.
- [12] S.K. Bains and PC. Banbury., "AC hopping conductivity and DLTS studies on electron-irradiated boron-doped silicon." Sem. Sci. Techn., 1987, 2 (1), pp. 20-29, DOI: 10.1088/0268-1242/2/1/003.
- [13] B. Cretu, E. Simoen, J.-M. Routoure, R. Carin, M. Aoulaiche, C. Claeys., "Low frequency noise spectroscopy in rotated UTBOX nMOSFETs", In Proceedings of ICNF'2015, IEEE DOI: 10.1109/ICNF.2015.7288588.
- [14] R. Talmat, H. Achour, B. Cretu, J.-M. Routoure, A. Benfdila, R. Carin, *et al.*, "Low frequency noise characterization in n-channel FinFETs", Solid State Electron., 2012, 70, pp. 20-26, DOI: 10.1016/j.sse.2011.11.007.